Numerical Simulation of Inward Solidification with Volume Change in Cylindrical Containers

Truong V. Vu

School of Transportation Engineering, Hanoi University of Science and Technology, No. 1 Dai Co Viet, Hai Ba Trung, Hanoi, Vietnam

Keywords: Inward Solidification, Cylinder, Front-Tracking, Volume Change, Triple Point

We use a front-tracking method to simulate inward solidification in a cylindrical container with volume change. The problem includes temporal evolution of three interfaces that meet at a triple point. The governing Navier–Stokes and energy equations are solved for the whole domain, setting the velocities in the solid phase to zero and with the non-slip condition on the solid–liquid interface. Computational results show that a cavity forms in the center of the cylinder if the density of solid is higher than that of liquid, i.e. $\rho_{sl} > 1.0$. In contrast, if $\rho_{sl} < 1.0$, the solidified product has a conical shape in the central region of the cylinder. The triple point also affects the solidification process as an increase in the growth angle results in a decrease in the cone angle at the top in the case of volume expansion.

Introduction

A solid–liquid phase change problem in which there is the presence of solid, liquid and gas appears in many methods of growing crystals from melts such as Czochralski crystal growth (Porrini, 2001), float-zone processing (Markvart, 2000) and laser welding (Booth, 2004). In these solidification processes, a tri-junction at which the three phases meet plays an important role in the formation of the solidified product. In addition, volume change caused by the density difference between solid and liquid can produce a curious shape (Ajaev and Davis, 2004).

The phase change problem including moving boundary during inward solidification from a cooled horizontal cylinder has received much attention (Riley *et al.*, 1974; Bilir and İlken, 2005). Experimental investigations can be found in Stewart and Smith (1987). Simplified analytical solutions of this problem have been presented by Riley *et al.* (1974), and Guenigault and Poots (1985).

Numerically, Tao (1967) developed a numerical method for the solidification problem of a saturated liquid contained in a cylindrical or spherical container. Voller and Cross (1981) presented an explicit technique based upon the enthalpy method to obtain the solidification and melting time for two-dimensional regions with cylindrical symmetry. Bilir and İlken (2005) used the enthalpy method with control volume approach to study the inward solidification in a cylindrical and spherical container with an initial temperature different from the fusion value.

Investigations accounting for volume change in the problem are rather limited. Viskanta and Gau (1982) adopted the integral and finite difference methods for the inward solidification in a horizontal tube. The authors also accounted for the effects of density difference on the solidification process. However, the effect of the tri-junction, i.e., presence of three phases, was not included.

A survey of experimental literature (Satunkin, 2003; Li *et al.*, 2011, 2012; Schmid *et al.*, 2012) leads us to recognize that volume change and the presence of three phases have strong effects on the solidification process. For instance, a cavity was found in the case of shrinkage (Allison and Pond, 1983; Assis *et al.*, 2009). For volume expansion, e.g., in the case of silicon, conical shapes were found [see Figure 2 in Li *et al.* (2011) and Figure 2 in Schmid *et al.* (2012)]. It is evident that the inward solidification process in cylindrical containers, which includes volume change and the presence of three phases, i.e. tri-junction effects, is extremely important both academically and in its industrial applications. However, it appears that numerical calculations are still lacking in the literature. These gaps motivate the present study on this problem.

Here, we apply the front-tracking/finite difference method for three-phase computations of solidification (Vu *et al.*, 2013, 2015) to simulate the inward solidification of pure phase change materials in cylindrical containers. We focus on the effects of the solid–to–liquid density ratio (volume change) and the growth angle (tri-junction condition) on the solidification process.

1. Mathematical Formulation and Numerical Method

Figure 1(a) shows the investigated problem, i.e., an axisymmetric solidification. A liquid with gas at temperature T_0 is placed in a circular cylinder. The fusion temperature of the liquid is T_m ($T_m \leq T_0$). At time $t = 0$, the cylinder temperature is suddenly lowered to T_c below T_m, i.e., $T_c < T_m$, and

Received on March 8, 2016; accepted on May 27, 2016
DOI: 10.1252/jcej.16we062
Correspondence concerning this article should be addressed to T. V. Vu (E-mail address: vvt_gago@yahoo.com).

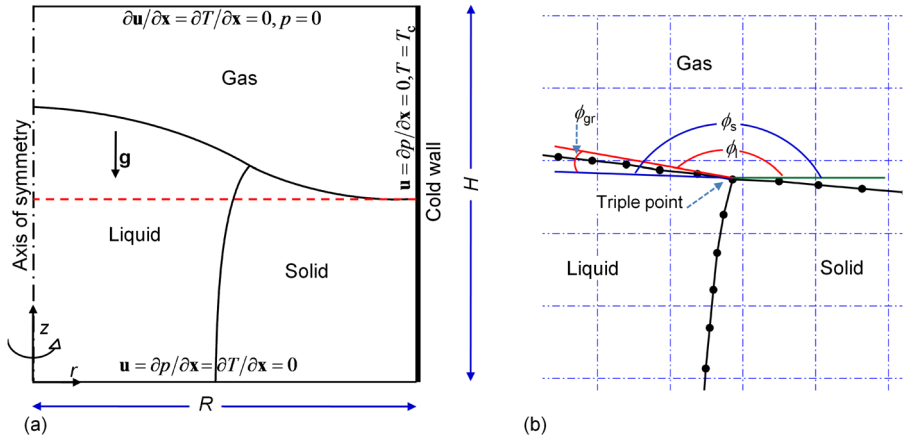

Fig. 1 Inward solidification in a cold tube: (a) computational domain and (b) front-tracking representation; in (a) the dash-line represents the initial liquid–gas interface

is kept at that temperature for $t>0$. A solid layer is formed near the cold wall, and then the solidification front propagates to the center of the cylinder. We assume that the fluids are incompressible, immiscible and Newtonian. We treat all phases as one fluid with variable properties such as density ρ, viscosity μ, thermal conductivity k and heat capacity C_p. In addition, volume change is assumed to occur only at the solidification front. In the case of volume expansion, the liquid is assumed to not flow over the top solid surface. Accordingly, the governing equations are given as Eqs. (1) to (3). The heat source at the solidification front $\dot{q}_f$ is given as Eq. (4).

$$\frac{\partial(\rho\mathbf{u})}{\partial t}+\nabla\cdot\rho\mathbf{u}\mathbf{u}=-\nabla p+\nabla\cdot[\mu(\nabla\mathbf{u}+\nabla\mathbf{u}^{\mathrm{T}})]+\int_f\sigma\kappa\delta(\mathbf{x}-\mathbf{x}_f)\mathbf{n}_f\mathrm{d}S+\rho\mathbf{g}[1-\beta(T-T_0)] \tag{1}$$

$$\frac{\partial(\rho C_pT)}{\partial t}+\nabla\cdot(\rho C_pT\mathbf{u})=\nabla\cdot(k\nabla T)+\int_f\dot{q}_f\delta(\mathbf{x}-\mathbf{x}_f)\mathrm{d}S \tag{2}$$

$$\nabla\cdot\mathbf{u}=(1/\rho_s-1/\rho_l)\int_f\delta(\mathbf{x}-\mathbf{x}_f)\dot{q}_f\mathrm{d}S/L_h \tag{3}$$

$$\dot{q}_f=k_s\left.\frac{\partial T}{\partial n}\right|_s-k_l\left.\frac{\partial T}{\partial n}\right|_l \tag{4}$$

Equation (3) accounts for volume change at the solidification front due to the density difference between solid and liquid (Vu *et al.*, 2013, 2015). The last term in Eq. (1) is the Boussinesq approximation for density changes due to thermal gradients (Gan *et al.*, 2003). The effect of the temperature on the surface tension force acting on the gas–liquid interface (Nas and Tryggvason, 2003) is given as Eq. (5).

$$\sigma=\sigma_0-\sigma_T(T-T_m) \tag{5}$$

Here, σ_0 and σ_T are the surface tension coefficient at a reference temperature T_m and the Marangoni tension coefficient.

We use here a front-tracking/finite difference method for the presence of three phases, phase change and volume change (Vu *et al.*, 2013, 2015). The interface is represented by connected elements that move on a fixed, rectangular grid (**Figure 1(b)**). The three phases and their properties are specified using indicator functions that are determined from known positions of the interface points: the points of the solidification and solid–gas fronts are used to construct the indicator I_s ($I_s=0$ in solid and $I_s=1$ in liquid and gas) while the indicator I_l ($I_l=0$ in liquid and solid and $I_l=1$ in gas) is built from the points on the solid–gas and liquid–gas interfaces. Accordingly, the values of the material property fields at every location are then given as Eq. (6).

$$\varphi=\varphi_gI_l+(1-I_l)[\varphi_lI_s+(1-I_s)\varphi_s] \tag{6}$$

Here, φ stands for ρ, μ, C_p, or k. I_s is also used to set the velocity field in the solid phase to zero. The solidification front propagates with the normal velocity V_n, $V_n=-\dot{q}_f/(\rho_sL_h)$, while the liquid–gas front is advected by the velocity interpolated from the fixed grid velocities.

At the triple point, we correct the position of this point by applying a constant growth angle $\phi_{gr}=\phi_s-\phi_l$, where ϕ_s and ϕ_l are the angles between the tangent to the solid–gas interface and the horizontal and between the tangent to the liquid–gas interface and the horizontal (see Figure 1(b)). We adjust the position of the triple point to satisfy the prescribed growth angle. A more detailed description of the method can be found in our previous works (Vu *et al.*, 2013, 2015).

2. Numerical Parameters

We choose the radius R of the cylinder as a scaling length, and $\tau_c=\rho_lC_lR^2/k_l$ as the characteristic time scale. The characteristic velocity scale is taken to be $U_c=R/\tau_c$.

With these above choices, the dynamics of the problem are governed by the following dimensionless parameters: Prandtl number $Pr=C_{pl}\mu_l/k_l$; Stefan number $St=C_{pl}(T_m-T_c)/L_h$;

Bond number $Bo=\rho_l gR^2/\sigma$; Weber number $We=\rho_l U_c^2 R/\sigma$; Rayleigh number $Ra=g\beta(T_m-T_c)R^3/(\nu_l\alpha_l)$; Marangoni number $Ma=\sigma_T R(T_m-T_c)/(\mu_l\alpha_l)$; initial dimensionless temperature of the liquid $\theta_0=(T_0-T_c)/(T_m-T_c)$; density ratios $\rho_{sl}=\rho_s/\rho_l$ and $\rho_{gl}=\rho_g/\rho_l$; viscosity ratio $\mu_{gl}=\mu_g/\mu_l$; thermal conductivity ratios $k_{sl}=k_s/k_l$ and $k_{gl}=k_g/k_l$; heat capacity ratios $C_{psl}=C_{ps}/C_{pl}$ and $C_{pgl}=C_{pg}/C_{pl}$; and expansion coefficient ratio $\beta_{gl}=\beta_g/\beta_l$. The temperature is non-dimensionalized as $\theta=(T-T_c)/(T_m-T_c)$. The dimensionless time is $\tau=t/\tau_c$.

As previously mentioned, in this study, we focus only on the effects of volume change (ρ_{sl}) and tri-junction conditions (ϕ_{gr}), and thus other parameters are kept constant, i.e., $Pr=0.01$, $St=0.1$, $Bo=10$, $Ma=300$, $We=1\times10^{-2}$, $Ra=1\times10^4$, $\theta_0=1.4$, $k_{sl}=1.0$, $k_{gl}=0.005$, $C_{psl}=C_{pgl}=1.0$, $\mu_{gl}=0.05$, and $\beta_{gl}=1.0$. The values of these parameters correspond to such materials as metal, silicon or germanium with R in the range of a few millimeters. The aspect ratio of the computational domain H/R is two with a grid resolution of 256×512.

Method validations have been extensively carried out in our previous works (Vu *et al.*, 2013, 2015), and thus are not presented in this paper.

3. Results and Discussion

Some materials, e.g., water and silicon, have a liquid phase denser than the solid phase, i.e. $\rho_{sl}<1.0$, while some others, e.g., *n*-octadecane and aluminum, have $\rho_{sl}>1.0$. This density difference causes volume change and affects the solidification process. **Figure 2** shows the predicted evolution of the solid–liquid and liquid–gas interfaces at $\tau=0.3$ and $\tau=1.8$ for three density ratios $\rho_{sl}=0.9$, 1.0, and 1.1. It can be seen that the evolution of the solidification front is strongly

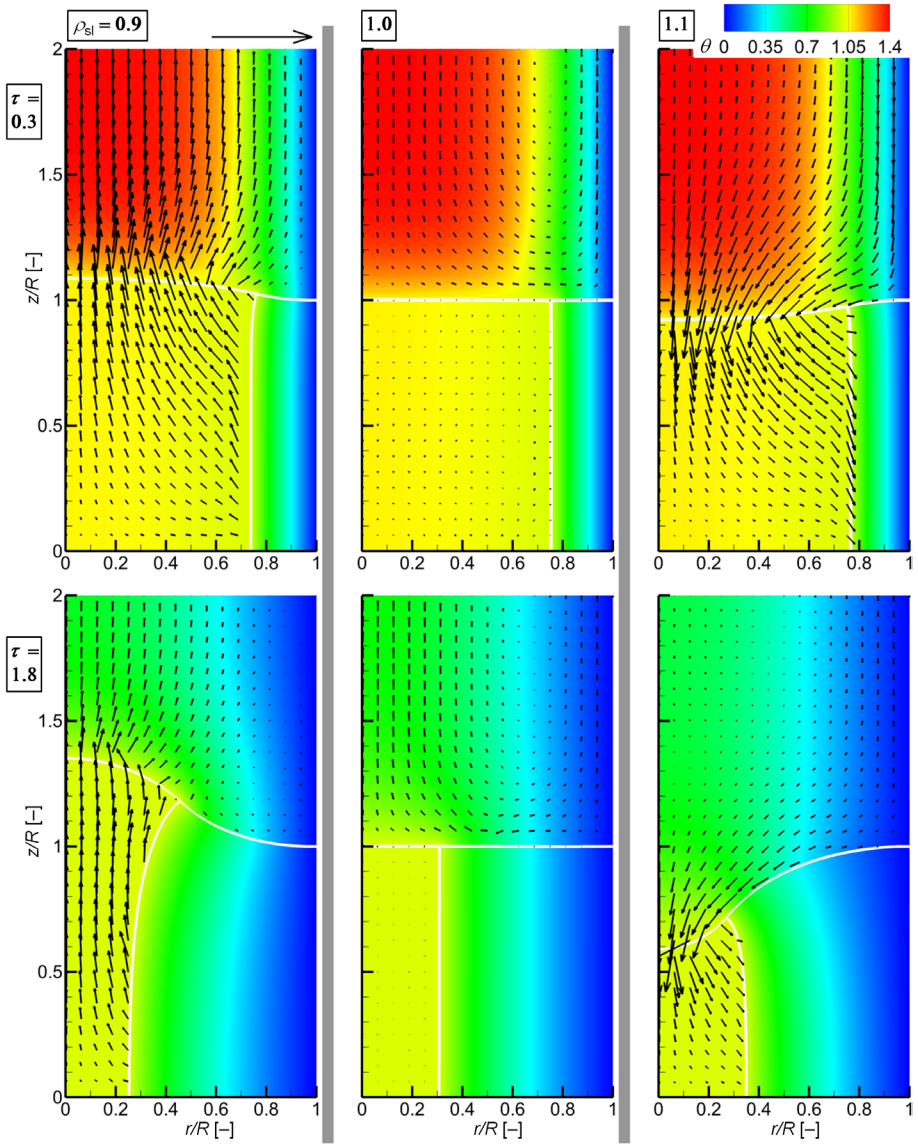

Fig. 2 Evolution of the solidification and liquid–gas fronts at time $\tau=0.3$ (upper) and $\tau=1.8$ (lower), for the density ratios $\rho_{sl}=0.9$ (left), 1.0 (middle) and 1.1 (right); the reference vector normalized by U_c has a value of 0.5; other parameters are shown in the text

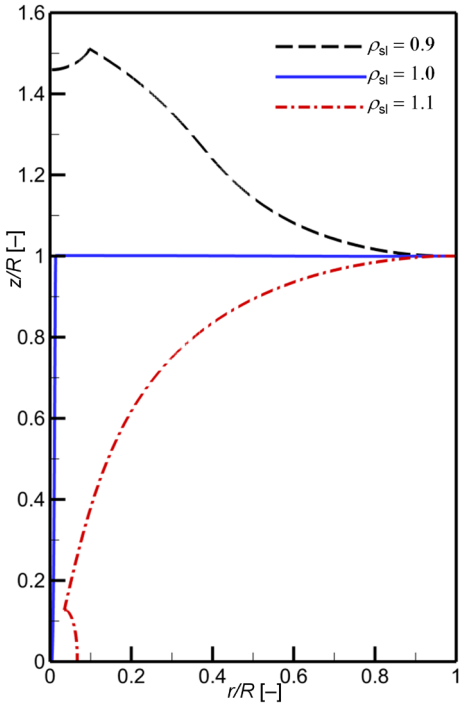

Fig. 3 The profiles of the nearly final stage of the solidification process for three different densities presented in Figure 2; other parameters are shown in the text

affected by the density change. For $\rho_{sl} = 0.9$ (the left frames in Figure 2), the density of the solid is lower than that of the liquid and this causes volume expansion upon solidification. The liquid flows away from the solid–liquid interface. This flow affects the liquid–gas interface and the circulation flow due to natural convection in the gas phase (as seen in the equal density case, i.e. the middle frames in Figure 2). The velocity field also indicates that the process tends to expand in the vertical direction rather than in the horizontal direction. Contrarily, the density ratio $\rho_{sl} = 1.1$ (the right frames in Figure 2) results in shrinkage upon solidification since the solid has a higher density than the liquid. The liquid flows toward the solidification interface to compensate. Accordingly, it reduces the liquid level as shown in Figure 2.

Figure 3 shows the shapes of the solid phase at the nearly final stage of solidification for these density ratios. It is evident that the volume change affects considerably the shape of the solidified product, i.e. expansion forming a cone, shrinkage forming a cavity near the axis of symmetry (Allison and Pond, 1983; Li *et al.*, 2011).

Next, we consider the effects of the tri-junction in terms of the grow angle. Reported experiments have yielded growth angles in the range of 0–28° for drop solidification (see Table 1 in Vu *et al.*, 2015). For instance, a zero growth angle is found for water (Anderson *et al.*, 1996), while those of silicon, germanium, and indium antimonide are respectively 12°, 14° and 25° (Satunkin, 2003). Accordingly, we investigate the effect of the growth angle by varying it in the range of 0–20° with $\rho_{sl} = 0.9$, as shown in **Figure 4**. For a zero grow angle $\phi_{gr} = 0°$, the solidified product forms a conical shape at the central region due to expansion. At higher ϕ_{gr}, the height of the solidified product increases. Accordingly, an increase in the growth angle results in a decrease in the cone angle at the top. This trend is similar to that for the drop solidification as reported in Vu *et al.* (2013, 2015).

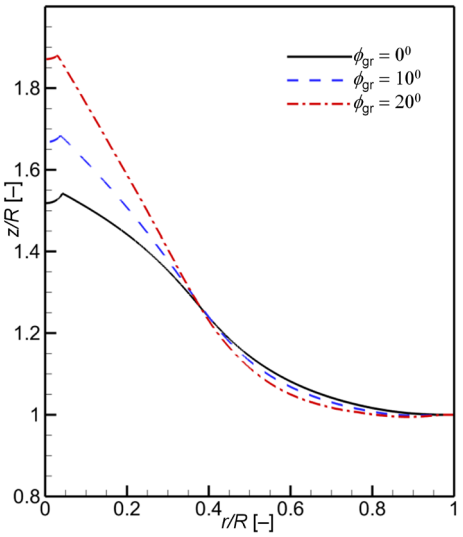

Fig. 4 The profiles of the nearly final stage of the solidification process for three different growth angles; other parameters are shown in the text

Conclusions

We have presented the simulation results of the inward solidification in a cylinder, with the effects of the density difference between the solid and liquid phases and of the tri-junction. The results were obtained by the front-tracking method (Vu *et al.*, 2013). Computational results show that volume change due to this density difference and the tri-junction have considerable effects on the shape of the solidified products. Expansion upon solidification, i.e. $\rho_{sl} < 1.0$, forms a conical shape near the axis of symmetry, while shrinkage, i.e., $\rho_{sl} > 1.0$, produces a cavity. In addition, with expansion, an increase in the growth angle results in a decrease in the cone angle at the top. These numerical calculations provide a valuable picture of how volume change and the tri-junction affect the inward solidification process, and help to understand more comprehensively about the formation of the cavity or conical shapes in the related experiments and industrial processes (Markvart, 2000; Assis *et al.*, 2009; Schmid *et al.*, 2012).

Acknowledgement

This research is funded by the Vietnam National Foundation for Science and Technology Development (NAFOSTED) under grant number 107.03-2014.21. The author is grateful to Prof. John C. Wells at Ritsumeikan University, Japan for facilitating computing resources.

Nomenclature

Bo	=	Bond number	[—]
C_p	=	specific heat capacity	[J/(kg K)]
$\mathbf{g}$	=	gravitational acceleration	[m/s^2]
H	=	computational domain height	[m]
I	=	indicator function	[—]
k	=	thermal conductivity	[W/(m K)]
L_h	=	latent heat of fusion	[J/kg]
Ma	=	Marangoni number	[—]
$\mathbf{n}$	=	unit normal vector	[—]
p	=	pressure	[N/m^2]
Pr	=	Prandtl number	[—]
q	=	heat flux	[W/m^2]
R	=	cylinder radius	[m]
Ra	=	Rayleigh number	[—]
S	=	surface	[m^2]
St	=	Stefan number	[—]
T	=	temperature	[K]
t	=	time	[s]
U_c	=	characteristic velocity	[m/s]
$\mathbf{u}$	=	velocity vector	[m/s]
V_n	=	solidification rate	[m/s]
We	=	Weber number	[—]
$\mathbf{x}$	=	position vector	[m]
α	=	thermal diffusivity	[m^2/s]
β	=	volumetric expansion coefficient	[K^{-1}]
δ	=	delta function	[m^{-3}]
ϕ	=	angle	[°]
κ	=	curvature	[m^{-1}]
μ	=	dynamic viscosity	[Pa s]
ν	=	kinematic viscosity	[m^2/s]
θ	=	dimensionless temperature	[—]
ρ	=	density	[kg/m^3]
σ	=	interfacial coefficient	[N/m]
τ	=	dimensionless time	[—]

‹Subscripts›

0	=	initial state
c	=	cold
f	=	interface
g	=	gas
gr	=	growth
h	=	hot
l	=	liquid
m	=	melting
s	=	solid

‹Superscript›

T	=	transpose

Literature Cited

Ajaev, V. S. and S. H. Davis; "The Effect of Tri-Junction Conditions in Droplet Solidification," *J. Cryst. Growth*, **264**, 452–462 (2004)

Allison, A. H. and R. B. Pond; "On Copying Bronze Statuettes," *Journal of the American Institute for Conservation*, **23**, 32–46 (1983)

Anderson, D. M., M. G. Worster and S. H. Davis; "The Case for a Dynamic Contact Angle in Containerless Solidification," *J. Cryst. Growth*, **163**, 329–338 (1996)

Assis, E., G. Ziskind and R. Letan; "Numerical and Experimental Study of Solidification in a Spherical Shell," *ASME J. Heat Transfer*, **131**, 024502–024502-5 (2009)

Bilir, L. and Z. İlken; "Total Solidification Time of a Liquid Phase Change Material Enclosed in Cylindrical/Spherical Containers," *Appl. Therm. Eng.*, **25**, 1488–1502 (2005)

Booth, H. J.; "Recent Applications of Pulsed Lasers in Advanced Materials Processing," *Thin Solid Films*, **453–454**, 450–457 (2004)

Gan, H., J. Chang, J. J. Feng and H. H. Hu; "Direct Numerical Simulation of the Sedimentation of Solid Particles with Thermal Convection," *J. Fluid Mech.*, **481**, 385–411 (2003)

Guenigault, R. and G. Poots; "Effects of Natural Convection on the Inward Solidification of Spheres and Cylinders," *Int. J. Heat Mass Transfer*, **28**, 1229–1231 (1985)

Li, T. F., K. M. Yeh, W. C. Hsu and C. W. Lan; "High-Quality Multi-Crystalline Silicon (mc-Si) Grown by Directional Solidification Using Notched Crucibles," *J. Cryst. Growth*, **318**, 219–223 (2011)

Li, T. F., H. C. Huang, H. W. Tsai, A. Lan, C. Chuck and C. W. Lan; "An Enhanced Cooling Design in Directional Solidification for High Quality Multi-Crystalline Solar Silicon," *J. Cryst. Growth*, **340**, 202–208 (2012)

Markvart, T.; Solar Electricity, 2nd ed., Wiley, New York, U.S.A. (2000)

Nas, S. and G. Tryggvason; "Thermocapillary Interaction of Two Bubbles or Drops," *Int. J. Multiphase Flow*, **29**, 1117–1135 (2003)

Porrini, M.; "Czochralski Silicon," Encyclopedia of Materials: Science and Technology, 2nd ed., pp. 1965–1970, Elsevier, Oxford, U.K. (2001)

Riley, D. S., F. T. Smith and G. Poots; "The Inward Solidification of Spheres and Circular Cylinders," *Int. J. Heat Mass Transfer*, **17**, 1507–1516 (1974)

Satunkin, G. A.; "Determination of Growth Angles, Wetting Angles, Interfacial Tensions and Capillary Constant Values of Melts," *J. Cryst. Growth*, **255**, 170–189 (2003)

Schmid, E., S. Würzner, C. Funke, V. Galindo, O. Pätzold and M. Stelter; "The Effect of the Growth Rate on the Microstructure of Multi-Crystalline Silicon," *J. Cryst. Growth*, **359**, 77–82 (2012)

Stewart, W. E. Jr. and K. L. Smith; "Experimental Inward Solidification of Initially Superheated Water in a Cylinder," *Int. Commun. Heat Mass Transf.*, **14**, 21–31 (1987)

Tao, L. C.; "Generalized Numerical Solutions of Freezing a Saturated Liquid in Cylinders and Spheres," *AIChE J.*, **13**, 165–169 (1967)

Viskanta, P. D. R. and C. Gau; "Inward Solidification of a Superheated Liquid in a Cooled Horizontal Tube," *Wärme- und Stoffübertragung*, **17**, 39–46 (1982)

Voller, V. R. and M. Cross; "Estimating the Solidification/Melting Times of Cylindrically Symmetric Regions," *Int. J. Heat Mass Transfer*, **24**, 1457–1462 (1981)

Vu, T. V., G. Tryggvason, S. Homma, J. C. Wells and H. Takakura; "A Front-Tracking Method for Three-Phase Computations of Solidification with Volume Change," *J. Chem. Eng. Japan*, **46**, 726–731 (2013)

Vu, T. V., G. Tryggvason, S. Homma and J. C. Wells; "Numerical Investigations of Drop Solidification on a Cold Plate in the Presence of Volume Change," *Int. J. Multiph. Flow*, **76**, 73–85 (2015)